NASA MEMO 2-22-59L

NASA

MEMORANDUM

SOME STATIC, OSCILLATORY, AND FREE-BODY TESTS OF BLUNT BODIES AT LOW SUBSONIC SPEEDS

By Jacob H. Lichtenstein, Lewis R. Fisher,
Stanley H. Scher, and George F. Lawrence

Langley Research Center
Langley Field, Va.

NATIONAL AERONAUTICS AND SPACE ADMINISTRATION
WASHINGTON
April 1959

NATIONAL AERONAUTICS AND SPACE ADMINISTRATION

MEMORANDUM 2-22-59L

SOME STATIC, OSCILLATORY, AND FREE-BODY TESTS OF BLUNT BODIES AT LOW SUBSONIC SPEEDS

By Jacob H. Lichtenstein, Lewis R. Fisher,
Stanley H. Scher, and George F. Lawrence

SUMMARY

Some blunt-body shapes considered suitable for entry into the earth's atmosphere were tested by both static and oscillatory methods in the Langley stability tunnel. In addition, free-fall tests of some similar models were made in the Langley 20-foot free-spinning tunnel.

The results of the tests show that increasing the flare of the body shape increased the dynamic stability and that for flat-faced shapes increasing the corner radius increased the stability. The test data from the Langley stability tunnel were used to compute the damping factor for the models tested in the Langley 20-foot free-spinning tunnel. For these cases in which the damping factor was low, -1/2 or less, the stability was critical and sensitive to disturbance. When the damping factor was about -2, damping was generally obtained.

INTRODUCTION

There is, at present, considerable interest being shown in body shapes which would be suitable for entry into the earth's atmosphere. Because of the wide range of conditions through which such a body would have to operate (for instance, Mach numbers from about 16 to less than 1), the design of bodies suitable for entry into the atmosphere has been complicated by the dearth of information existing for blunt bodies of low fineness ratio under these conditions. In order to obtain some idea of the magnitude of the directional stability and damping of some typically shaped blunt bodies, static and oscillation tests were made at low speeds in the Langley stability tunnel. The oscillation tests gave a measure of the directional stability and the damping in yaw through an angle-of-attack range from 0° to 12° for 13 basic configurations. The static tests gave a measure of the lift, drag, and pitching moment. In addition to the tests, a comparison is made between the estimated behavior

of several of the bodies, based upon a two-degree-of-freedom consideration using the stability derivatives obtained from the stability-tunnel tests, and the free-fall behavior observed for some comparable models in the Langley 20-foot free-spinning tunnel.

SYMBOLS

The test data from the Langley stability tunnel are presented in the form of standard coefficients about a pivot point indicated for each model (roughly one-third of the length back of the nose). The angular deflections are shown in figure 1. The symbols used are defined as follows:

A	maximum cross-sectional area, sq ft
C_D	drag coefficient, $\frac{\text{Drag}}{QA}$
C_L	lift coefficient, $\frac{\text{Lift}}{QA}$
C_{L_α}	lift-curve slope, $\frac{\partial C_L}{\partial \alpha}$, per radian
C_m	pitching-moment coefficient, $\frac{\text{Pitching moment}}{QAd}$
C_{m_q}	damping-in-pitch parameter, $\frac{\partial C_m}{\partial \frac{qd}{2V}}$
C_{m_α}	static stability parameter, $\frac{\partial C_m}{\partial \alpha}$, per radian
C_n	yawing-moment coefficient, $\frac{\text{Yawing moment}}{QAd}$
C_{n_r}	damping-in-yaw parameter, $\frac{\partial C_n}{\partial \frac{rd}{2V}}$
C_{n_ψ}	directional stability parameter, $\frac{\partial C_n}{\partial \psi}$, per radian

C_Z normal-force coefficient, $\frac{-\text{Normal force}}{QA}$

C_{Z_α} normal-force slope, $\frac{\partial C_Z}{\partial \alpha}$, per radian

$D = \frac{d}{dt}$

d maximum diameter of body without flares, ft

f angular frequency, $\frac{\omega}{2\pi}$, cps

I_Y moment of inertia, slug-ft^2

l model length, ft

m mass of body, slugs

Q dynamic pressure, $\frac{1}{2}\rho V^2$, lb/sq ft

q pitching velocity, $\frac{\partial \theta}{\partial t}$, radians/sec

r yawing velocity, $\frac{\partial \psi}{\partial t}$, radians/sec

$\frac{qd}{2V}$ pitching-velocity parameter referred to diameter

$\frac{rd}{2V}$ yawing-velocity parameter referred to diameter

t time, sec

V free-stream velocity, ft/sec

x distance from nose of model measured along longitudinal body axis, ft

α angle of attack, deg

θ angular displacement of longitudinal axis from a fixed reference axis

ρ mass density of air, slugs/ft^3

ψ angle of yaw, radians

ω angular velocity, radians/sec

A dot above a symbol denotes the derivative with respect to time; a double dot denotes a second derivative with respect to time.

MODELS, APPARATUS, AND TESTS

Models

The models used in the Langley stability tunnel consisted of the 13 basic bodies of revolution shown in figure 2. Several of these were modified by inclusion of nose rings, skirts, bands, waists, or fins. These modifications also are shown in figure 2. Photographs of the models are shown in figure 3. The pivot center was located at 1/3 of the model length rearward of the nose $\left(3\frac{1}{16}\text{ inches}\right)$ for models 1, 2, 3, 4, 5, 6, and 7. The same pivot-point location was used for all the other models except the cone (model 13); therefore, as the model length varied, the relative center-of-gravity location changed. For models 11 and 12, a relative center-of-gravity location of $0.57l$ also was tried. For the cone, the pivot point could not be moved any closer to the nose than $0.45l$ because of space limitations within the model.

The stability-tunnel models were turned from mahogany blocks; the outside surface was sanded smooth, shellacked, and polished.

The models used in the spin-tunnel tests were made of a thin shell of fiberglass. Weights were added to give the indicated center-of-gravity locations and mass characteristics. Sketches of the models used in the spin-tunnel tests are shown in figure 4. Models A, C, and model A with the band which were used in the spin-tunnel tests are the same shapes as models 11 and 12 and model 11 with the band which were used in the stability-tunnel tests.

Apparatus

The oscillation and data recording apparatus are shown in figure 5. The apparatus was mounted on a sting support in the 6- by 6-foot test section of the Langley stability tunnel. The oscillation apparatus consisted of a piece of Swedish blue spring steel 1/32 inch thick and 6 inches wide which was held between clamps so that there was only a 1/16-inch gap between the part fixed to the sting and the part fixed to the model. Thus, the pivot axis was defined. A pointer attached

to the back of the model oscillated with it just above a graduated protractor. A 16-millimeter movie camera mounted above the tunnel was used to photograph the motion of this pointer and the face of a stopwatch so that the period of the oscillation could be determined.

Stops to limit the motion to about ±5° were provided to prevent the flex pivot from being damaged in case instability was encountered.

The static tests used a three-component strain-gage balance which gave the normal force, axial force, and pitching moment; the strain-gage balance was mounted on the sting in place of the oscillation apparatus.

Tests

Both static tests and oscillation-in-yaw tests were made in the Langley stability tunnel. The static tests were made through an angle-of-attack range from 0° to 16° in 2° increments. The oscillation tests were of the free-decay type in which the model was free to oscillate in yaw under the influence of only the aerodynamic forces and the restraint of the flexure plate. The oscillation was initiated by holding the model cocked against one of the stops and then suddenly releasing the model. The movie camera photographed the movement of the pointer at the rear of the model and the stopwatch so that the period and rate of decay of the oscillation could be measured. The tests were made in most cases for angles of attack of 0°, 4°, 8°, and 12° and at a dynamic pressure of 24.9 pounds per square foot which corresponds to a Mach number of 0.13 and a Reynolds number of about 0.92×10^6 based upon the diameter d. In addition to the wind-on tests, wind-off tests also were made to evaluate the contribution of the flexure to the period and damping. Most of the tests were made with the back of the model closed as much as possible, still permitting the model to oscillate about ±5°.

The spin-tunnel tests were observation tests. The model was introduced into the vertically rising airstream and the speed of the airstream varied so that the drag balanced the weight. The resulting behavior of the free model was observed and photographed by 16-millimeter movie cameras so that some measure of the amplitude and frequency could be obtained.

PRESENTATION OF RESULTS

The data for related models are presented together. Thus, the static test data for models 1, 2, and 3, which are similar except

for flare angle, are presented in figure 6(a). The static-test data for models 4, 5, 6, and 7, which are similar except for nose shape, are presented in figure 6(b). The static-test data for models 8, 9, and 10, which differ only in the flare of the skirt, are presented in figure 7(a). The static-test data for models 11, 12, and 13, which are odd shapes, have been grouped together in figure 7(b).

The oscillatory damping-in-yaw data are presented in a manner similar to that used for the static-test data. The data for models 1, 2, and 3 are grouped together in figure 8. The data for models 4, 5, 6, and 7 are presented in figures 9(a) and (b); the data for models 8, 9, and 10 are presented in figure 9(c). The data for the odd models 11, 12, and 13 are presented in figure 10. A comparison of the static-test values of C_{m_α} and oscillatory-test values of C_{n_ψ} at zero angle of attack is shown in table I.

The data from the spin-tunnel tests are presented in table II together with a damping factor and an estimated frequency computed from data obtained from the stability-tunnel tests.

DISCUSSION

Static Tests

Examination of the data in figure 6 shows that, if the nose of the body is rounded, generally there is a positive lift-curve slope which is comparatively straight, a lower drag coefficient, and a stable pitching-moment variation.

It should be noted that except for the sphere the differences in lift and pitching moment at $\alpha = 0^\circ$ for the various model configurations are probably due to some asymmetry of the model configuration. For the sphere, these variations are probably due to fluctuations of the separation points.

Effect of flare angle.- Changing the flare angle of the body (fig. 6(a)) had only a minor effect on the general characteristics of a round-nose body. The data do show, however, that increasing the flare angle was detrimental. The waist modification made to model 2 decreased the lift-curve slope and pitching-moment slope and increased the drag.

For model 3, however, the waist modification increased the lift-curve slope and pitching-moment slope and decreased the drag at low angles of attack, but at the higher angles of attack these advantages were abrogated and even reversed.

Effect of nose corner shape.- The data in figure 6(b) show the drastic effects that variations in the corner treatment can produce. A model with a reasonably large radius, model 7, exhibited results similar to the round-nose models. The small-radius models, models 4, 5, and 6, showed a lift slope of opposite sign (negative slope), a large increase in drag, and a large decrease in static stability. The progressive change from a small positive corner radius to a small negative corner radius (radii on models 5, 4, and 6) showed progressive adverse effects.

It should be mentioned that these results are apparently sensitive to Reynolds number and can be significantly altered by changes in Reynolds number as indicated in reference 1.

Effect of skirt flare.- The data in figure 7(a) show that increasing the flare of the skirt generally improved the lift and pitching-moment characteristics. It also tended to decrease the drag at low angles of attack but increased the drag at higher angles of attack. It is interesting to note that for similar models the increase in length of model 8 over that of model 5 (about 25 percent) resulted in a lower drag. (Compare figs. 6(b) and 7(a).) Note also that in the case of model 9, which has the smaller flare, the flare is practically ineffective at low angles of attack and the lift and pitching moments are approximately the same as those for model 8 with no flare. At the high angles of attack, however, the lower portion of the flare becomes effective; a large positive increment in lift and a negative increment in pitching moment then occur with the result that the data approach those for model 10.

Additional models.- The data in figure 7(b) for the reversed flare shape (model 11) show variations with angle of attack similar to those for the flared models (models 1, 2, and 3) although the lift slope, drag, and static stability values were lower. It is interesting to note that this was the only configuration tested that had a drag coefficient lower than that of the sphere (model 12).

The unstable nature of the flow about a sphere (model 12) is shown to some extent by the large difference in values for the lift and pitching moments obtained on two separate occasions at zero angle of attack. (See fig. 7(b).) This effect also existed at higher angles of attack but to a smaller degree because the edge of the truncated section tends to stabilize the flow at the back of the sphere by fixing separation.

The data for the cone (model 13, fig. 7(b)) exhibited the positive lift slope, stable pitching moment, and high-drag characteristics usually expected for a cone.

Oscillation Tests

As mentioned previously, tests were made with the back of the model both open and closed. A missile nose, however, will have the back closed in some form, and therefore the more pertinent tests are considered to be those with the back closed. The back-open results are presented only to illustrate the effect of some configuration change that was not tested with the back closed.

Effect of flare angle.- The data in figure 8 for the three models with the same spherical nose but different flare angles (models 1, 2, and 3) show that the increase in flare angle tended to decrease the static directional stability slightly but appreciably increased the damping in yaw. The effect of increasing the flare angle until the configuration approaches a cone can be surmised from the results of model 13 (fig. 10(a)), which is a cone with a somewhat larger flare angle than model 3. The data indicate a slight improvement in static stability and a considerable improvement in damping in yaw.

Two modifications were tested on both models 2 and 3. In one case the models were modified to have a waist and in the other case, four tail fins were added. The surprising difference of such similar modifications to the two models can be seen in figures 8(b) and 8(c). For model 2 the waist modification decreased the static stability slightly but increased the damping in yaw. For model 3 the waist modification decreased the damping in yaw to such a point that the model was dynamically unstable. The tests to find the effect of tail fins were made with the back of the model open. The addition of four tail fins tended to increase the static stability for both models 2 and 3. For model 2 the damping in yaw was increased at low angles of attack; at the higher angles of attack the damping in yaw was actually decreased. For model 3, however, the fins appeared generally to have a beneficial effect on the damping in yaw.

Effect of nose corner shape.- The effect of changes in the nose-corner configurations, models 4, 5, 6, and 7, is shown in figure 9(a). The data show that the relatively sharp-corner configurations, models 4, 5, and 6, were for the most part dynamically unstable (negative damping). Only for the model with an appreciable corner radius, model 7, was any reasonable damping obtained.

For two of the models, models 4 and 5, some rather sketchy tests indicated that additions of four tail fins improved the damping considerably.

Effect of skirt flare.- The data for models 8, 9, and 10 presented in figure 9(c), show the effect of the skirt flare. The model without any skirt flare, model 8, was unstable at low angles of attack but showed good damping at the high angles of attack. Increasing the skirt flare made the models dynamically unstable.

Additional models.- The data for the odd models, models 11, 12, and 13, presented in figure 10 show that model 11 was stable with a small amount of damping whereas model 12 was unstable. Addition of a band to model 11 increased the directional stability slightly but had a negligible effect on the damping. Installation of four tail fins, however, improved the directional stability and damping. Moving the center of gravity rearward generally had a detrimental effect on the stability and damping. For model number 12, however, either the addition of a band, tail fins, or moving the center of gravity rearward seemed to have a beneficial effect within portions of the angle-of-attack range.

Comparison of Static Stability Parameter Obtained From Static and Oscillation Tests

For the bodies of revolution, the static stability derivatives C_{m_α} and C_{n_ψ} should be the same at zero angle of attack. A comparison of values of C_{m_α} measured during the static tests and comparable values of C_{n_ψ} measured during the oscillation tests is shown in table I. It can be seen that, in general, the oscillatory values of C_{n_ψ} are somewhat lower than the static values of C_{m_α}. For the oscillatory cases marked unstable, the instability may be due to negative damping rather than an unstable value of C_{n_ψ}.

Comparison of Indicated and Observed Behavior

Before discussing these results, it should be mentioned that the computed damping factor is limited to a comparatively narrow angle-of-attack band; thus, only the cases in which the model was launched nose down are comparable. The method of computing the damping factor is given in the appendix. Comparison of the observed behavior of a model in the spin tunnel with the expected behavior of the model based upon the computed damping factor indicates a good qualitative agreement. (See table II.) When the damping factor was large (about -2.0), good damping was indicated and the tests for comparable models (models B

and D) showed no oscillation. When the damping factor was relatively small (about -1/2 or less), low damping was indicated and the comparable model (model A) oscillated through an appreciable amplitude or was unstable. Although the computed damping factor indicated that some damping existed, these cases apparently are just marginal and therefore minor disturbances (for example, those arising from a slightly irregular or unsteady airstream) could induce an oscillation or even unstable behavior. For the sphere (models C and 12) both the spin- and stability-tunnel tests indicated unstable behavior.

CONCLUDING REMARKS

Some blunt bodies considered suitable for entry into the earth's atmosphere were tested by static, oscillatory, and free-body methods at low speeds to determine the stability of these bodies. The results showed that increasing the flare angle of the body generally increased the dynamic stability. On a flat-front body, the nose corner shape was found to have a very important effect upon the stability of the body. Increasing the corner radius (from a small negative radius to a small positive radius) tended to increase the static stability and an appreciable corner radius was necessary to obtain reasonable damping. A comparison of the damping factor and frequency computed by using the test data with the behavior of the models in the free-body tests indicated that when the damping factor was low, about -1/2, the behavior of the configuration was critical and the stability would be very sensitive to disturbances. When, however, the damping factor was relatively large, about -2, good damping was generally obtained.

The Reynolds number for the tests reported herein was very low in comparison with the actual full-scale values. It is recognized therefore that there may be an appreciable Reynolds number effect. For those shapes which have separation on the forward portion of the body, the Reynolds number effect may change the nature and amount of reattachment on the rearward portion of the body.

Langley Research Center,
National Aeronautics and Space Administration,
Langley Field, Va., November 28, 1958.

APPENDIX

METHOD OF COMPUTING THE DAMPING FACTOR

In order to compute the damping factor, a two-degree-of-freedom system was considered using the following normal-force and pitching-moment equations:

For the normal force

$$m\dot{\alpha} + m\dot{\theta} - \frac{QA}{V} C_{Z_\alpha} \alpha = 0 \tag{A1}$$

For the pitching moment

$$I_Y\ddot{\theta} + QAdC_{m_\alpha}\alpha - \frac{QAd^2}{2V} C_{m_q}\dot{\theta} = 0 \tag{A2}$$

If $D = \frac{d}{dt}$ and $D^2 = \frac{d^2}{dt^2}$ and if equations (A1) and (A2) are put in determinant form and then expanded, the following equation results:

$$D^2 - \frac{QA}{V}\left(\frac{C_{Z_\alpha}}{m} + \frac{d^2C_{m_q}}{2I_Y}\right)D + \frac{QAd}{mI_Y}\left(\frac{QAd}{2V^2} C_{Z_\alpha}C_{m_q} - mC_{m_\alpha}\right) = 0 \tag{A3}$$

which is of the form

$$D^2 + bD + c = 0$$

and the solution for D is

$$D = -\frac{b}{2} \pm \sqrt{\left(\frac{b}{2}\right)^2 - c} \tag{A4}$$

If we assume that the solution to the original equations (eqs. (A1) and (A2)) is of the form

$$\alpha = A_o e^{\lambda t} \quad \text{or} \quad \dot{\theta} = B_o e^{\lambda t}$$

where A_o and B_o are constants depending upon the initial conditions, it can be shown that the term $-\frac{b}{2}$ from equation (A4) is the damping factor in the final solution and that the frequency in radians per second is given by the $\sqrt{c - \left(\frac{b}{2}\right)^2}$ term. The damping factor therefore is

$$\text{Damping factor} = \frac{QA}{2V}\left(\frac{C_{Z_\alpha}}{m} + \frac{d^2 C_{m_q}}{2I_Y}\right) \tag{A5}$$

The frequency is given as follows:

$$\omega = \sqrt{\left[\frac{QAd}{mI_Y}\left(\frac{QAd}{2V^2} C_{Z_\alpha} C_{m_q} - mC_{m_\alpha}\right)\right] - \left[-\frac{QA}{2V}\left(\frac{C_{Z_\alpha}}{m} + \frac{d^2 C_{m_q}}{2I_Y}\right)\right]^2} \tag{A6}$$

The frequency in cycles per second is

$$f = \frac{\omega}{2\pi}$$

For models A and C used in the spin-tunnel tests, there were comparable models for the stability-tunnel tests; however, for models B and D there was no exact counterpart. The stability derivatives therefore had to be estimated from the data for the most nearly representative shapes. For model B, a combination of data from models 2 and 3 of the stability-tunnel program was used and for model D the data from model 2 were used.

Because the spin-tunnel and stability-tunnel tests were not made with the same center-of-gravity locations, it was necessary to correct the C_{m_α} and C_{m_q} measurements to the center-of-gravity location used in the free-model tests. For conversion of the C_{m_α} term, the following expression was used:

$$C_{m_\alpha} = \left(C_{m_\alpha}\right)_{\text{stab. tunnel}} + C_{L_\alpha} \frac{\Delta x}{d} \tag{A7}$$

and for conversion for the damping term C_{m_q} the following expression was used:

$$C_{m_q} = \left(C_{m_q}\right)_{\text{stab. tunnel}} + C_{L_\alpha}\left(\frac{\Delta x}{d}\right)^2 \qquad \text{(A8)}$$

where the term Δx is the distance between the center-of-gravity location for the stability-tunnel tests and that for the spin-tunnel tests.

Equation (A8) was used to obtain the appropriate damping coefficient C_{m_q} to be used in equation (A5) for evaluating the damping factor.

REFERENCE

1. Polhamus, Edward C.: Effect of Flow Incidence and Reynolds Number on Low-Speed Aerodynamic Characteristics of Several Noncircular Cylinders With Applications to Directional Stability and Spinning. NACA TN 4176, 1958.

TABLE I.- COMPARISON OF STATIC TEST VALUES OF C_{m_α} WITH OSCILLATORY TEST VALUES OF C_{n_ψ} AT $\alpha = 0^\circ$

Model	C_{m_α}, per radian	C_{n_ψ}, per radian
1	-0.52	-0.38
2	-.33	-.26
2 modified	.05	-.23
3	-.40	-.28
3 modified	-1.18	Unstable
4	0	--------
5	0	--------
6	-.18	--------
7	-.56	-.43
8	-.13	Unstable
9	-.50	Unstable
10	-1.98	Unstable
11	-.22	-.28
12	.65 -.46	Unstable
13	-.46	-.30

TABLE II.- TEST RESULTS OF ENTRY NOSE SHAPES IN FREE-SPINNING TUNNEL AND COMPUTED DAMPING FACTORS AND FREQUENCY

Model configuration (see fig. 4)	Model weight, grams	Center-of-gravity location rearward from nose, percent l	Method of launching	Test results				Computed results	
				Approximate rate of descent, ft/sec	Drag coefficient	Behavior in descent	Oscillation frequency, cps	Damping factor, $-\frac{b}{2}$	Oscillation frequency, cps
A	588.5	21.6	Released nose down	81	0.7050	Oscillated ±25°	2.0	-0.50	2.7
A	588.5	21.6	Tumbling about lateral axis	69	------	Continued tumbling	---	--------	---
A	588.5	41.9	Released nose down	69	------	Tumbled	---	-.42	---
A	588.5	41.9	Released nose up	69	------	Tumbled	---	--------	---
A	588.5	74.9	Released nose down	84	------	Turned nose up and oscillated ±60° to 90°	---	-.01	---
A	588.5	74.9	Released nose up	84	------	Oscillated ±60° to 90°	---	--------	---
A	588.5	74.9	Tumbling	84	------	Stopped tumbling, turned nose up, and oscillated ±60° to 90°	---	--------	---
A with $\frac{1}{2}$-in. band	607	21.6	Released nose down	86.9	.6273	Oscillated ±15°	---	--------	---
A with $1\frac{1}{4}$-in. band	631	21.6	Released nose down	>100	------	Oscillated ±15°	2.2	>-.60	3.4
B	172	47.4	Released nose down	100	.305	Nose down, no oscillation	---	-2.32	---
B	172	47.4	Released nose up	<100	------	Tumbled	---	--------	---
C	313	37.1	Released nose down	68	------	Oscillated and rotated until started spinning rapidly about a vertical tunnel axis while at 90° angle of attack	---	Unstable	---
C	313	48.9	Released nose down	68	------	Turned nose up, rotated about longitudinal axis while traveling around periphery of tunnel	---	Unstable	---
C	313	70.2	Released nose down	68	------	Same as for center-of-gravity location at 0.4891	---	--------	---
D	48	41.5	Released nose down	49.3	.4197	Nose down, no oscillation	---	-1.90	---
D	48	41.5	Tumbling about lateral axis	32.5	------	Continued tumbling	---	--------	---
D	48	41.5	Released nose up	35.9	------	Falling-leaf motion, oscillated ±20° from nose-up attitude	---	--------	---
D	78	29.5	Released nose down	63.2	.3963	Nose down, no oscillation	---	-1.84	---
D	78	29.5	Tumbling about lateral axis	40.0	------	Continued tumbling	---	--------	---
D	78	29.5	Released nose up	40.0	------	Tumbled	---	--------	---
D	78	29.5	Nose up with rotation applied about longitudinal axis	40.0	------	Tumbled after applied rotation damped out	---	--------	---

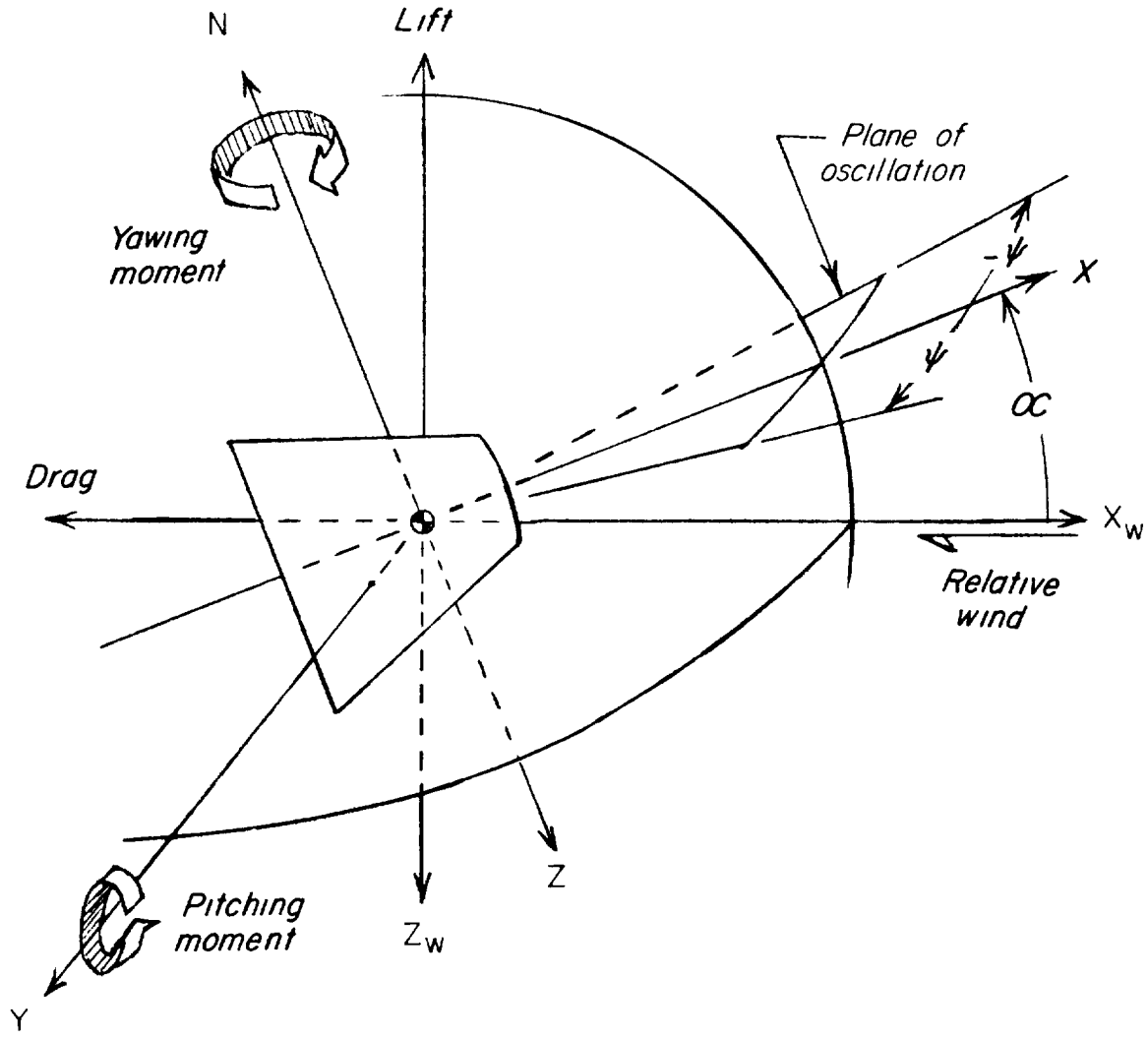

Figure 1.- System of axes used. Arrows indicate positive direction of forces, moments, angles, and angular velocities.

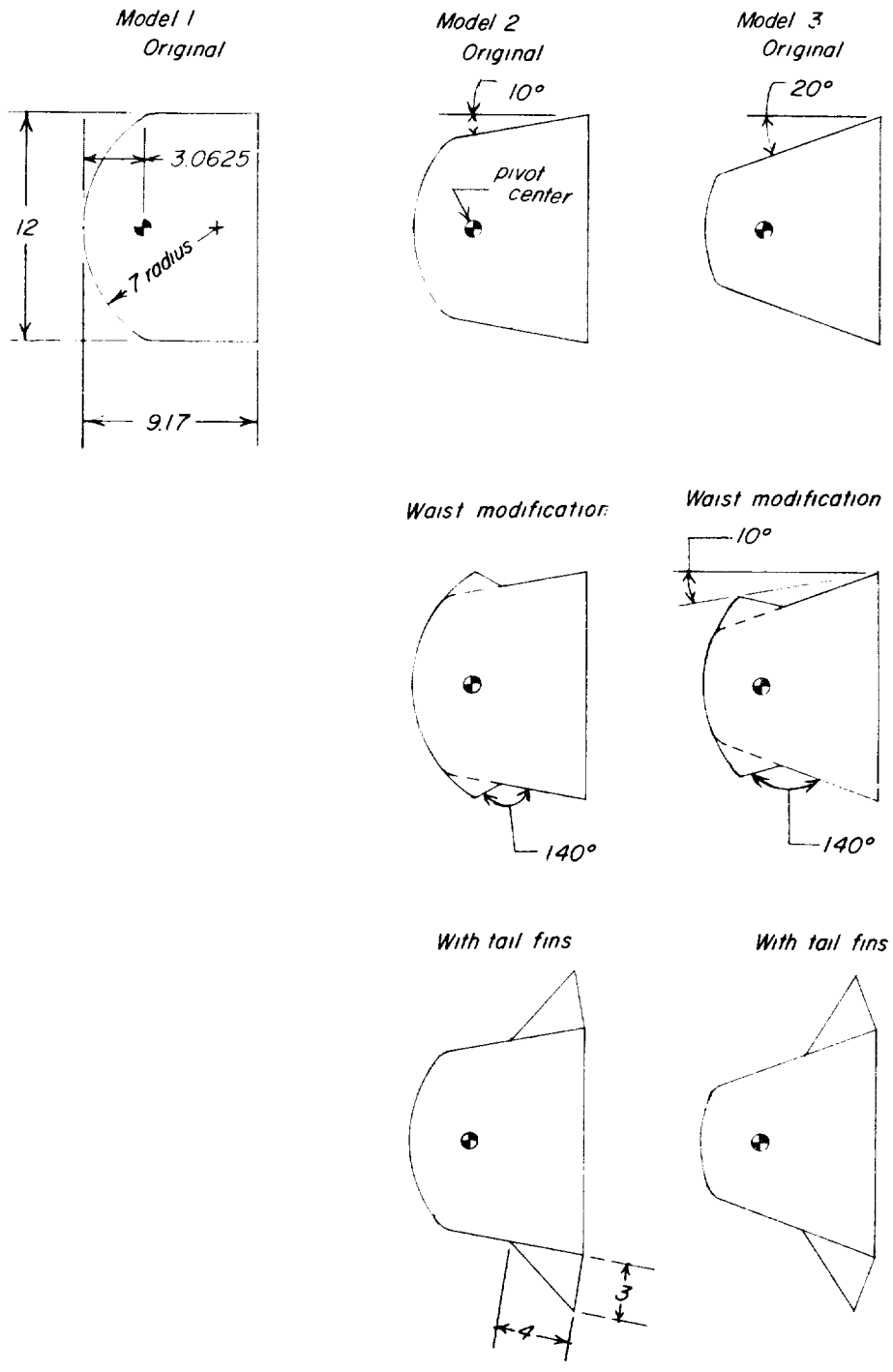

Figure 2.- Sketches of models tested in the Iangley stability tunnel. Original configurations and modified configurations. All dimensions are in inches.

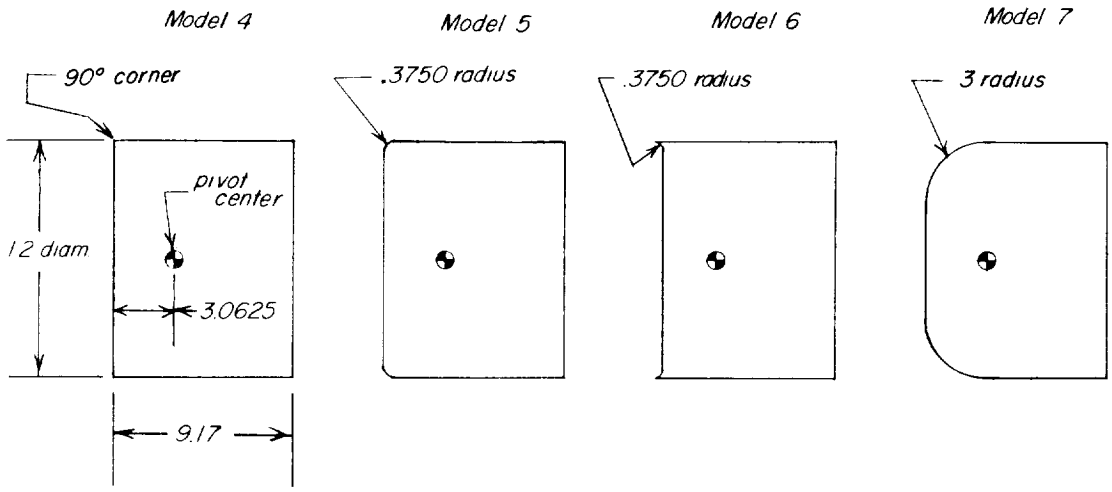

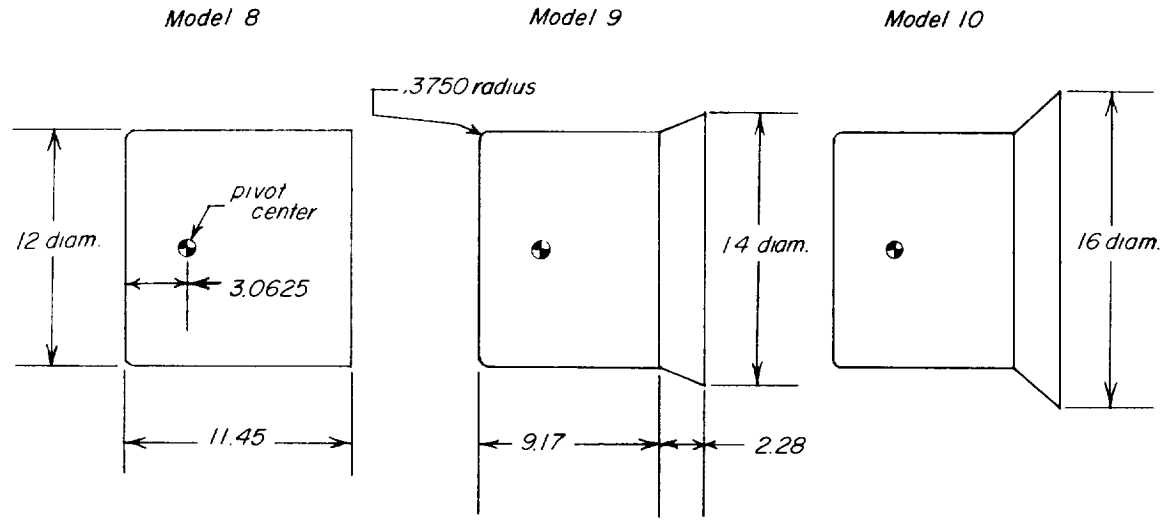

Figure 2.- Continued.

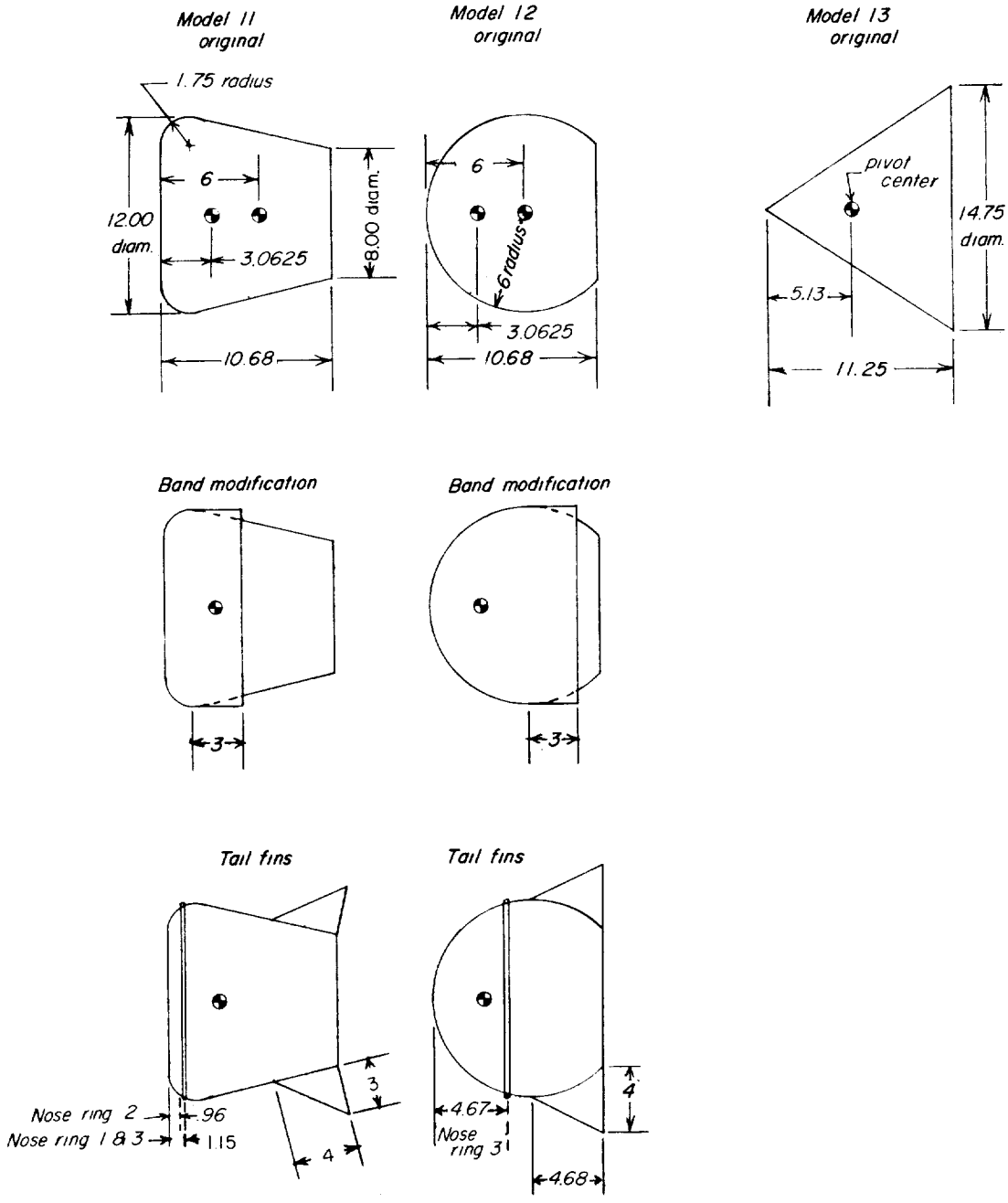

Nose-ring location shown on model with fins for illustration although tested individually. Nose rings 1 and 2 made of 1/16-in. diameter wire; nose ring 3 made of 1/8-in. diameter wire.

Figure 2.- Concluded.

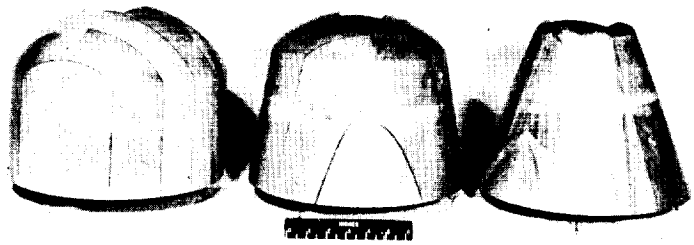

Model 1 Model 2 Model 3

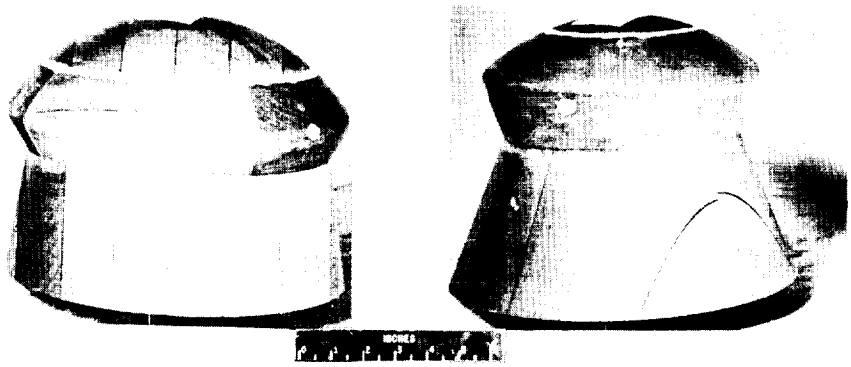

Model 2 with waist modification

Model 3 with waist modification

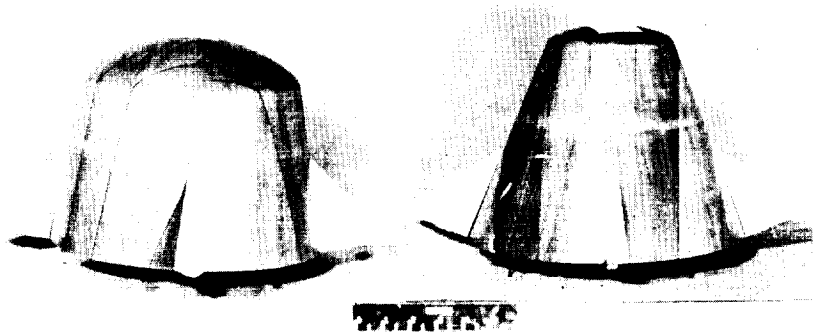

Model 2 with fins

Model 3 with fins

L-58-172a

(a) Models 1, 2, and 3 (original and modified configurations).

Figure 3.- Photographs of the models tested in Langley stability tunnel.

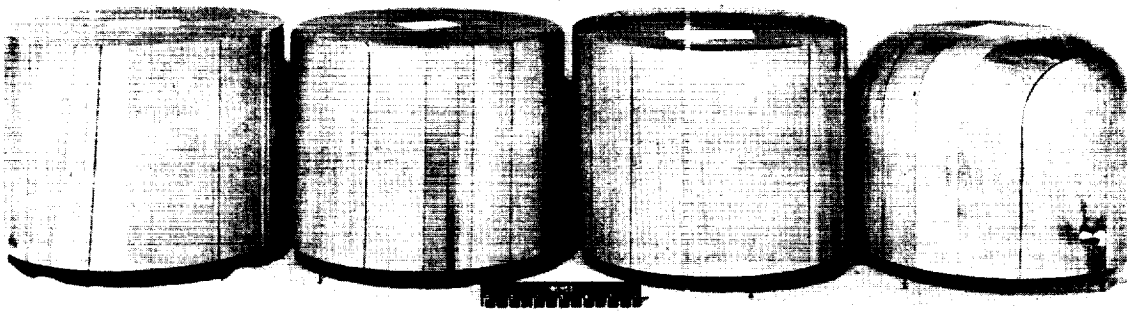

Model 4 Model 5 Model 6 Model 7

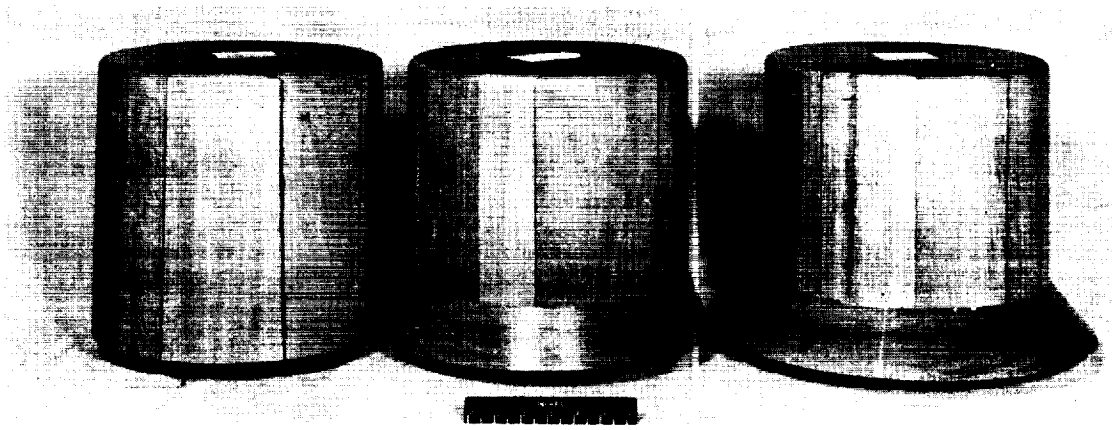

Model 8 Model 9 Model 10

(b) Models 4, 5, 6, 7, 8, 9, and 10. L-58-173a

Figure 3.- Continued.

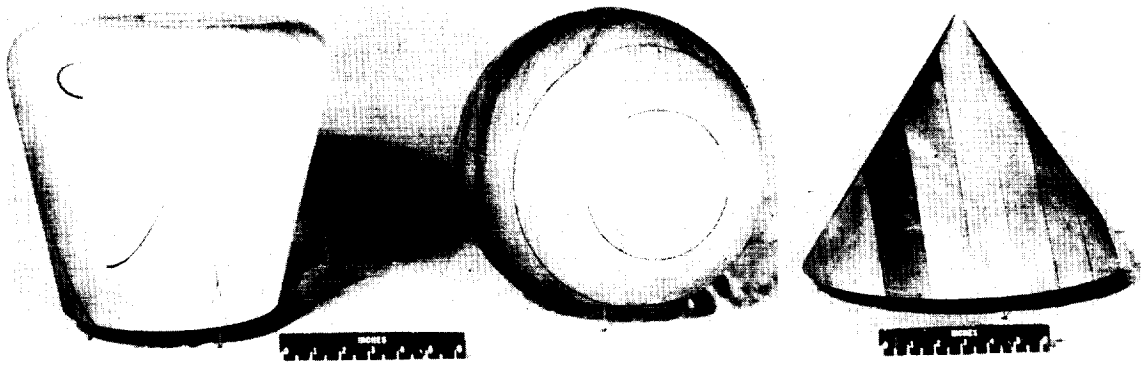

Model 11 Model 12 Model 13

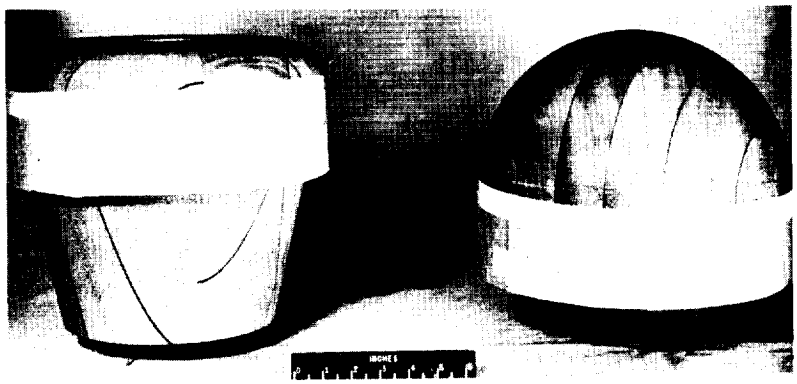

Model 11 with band Model 12 with band

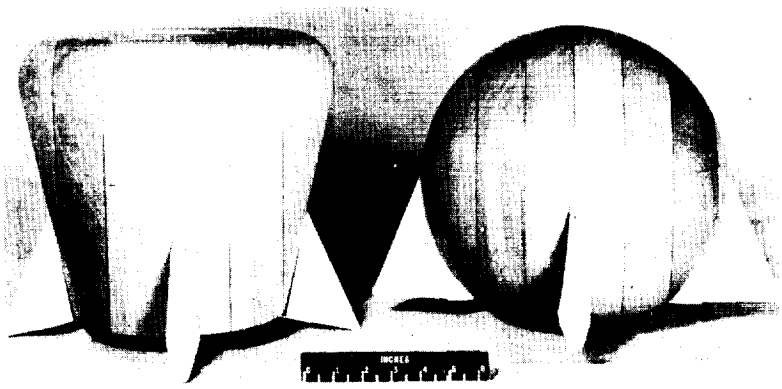

Model 11 with fins Model 12 with fins

L-58-174a

(c) Models 11, 12, and 13 (original and modified configurations).

Figure 3.- Concluded.

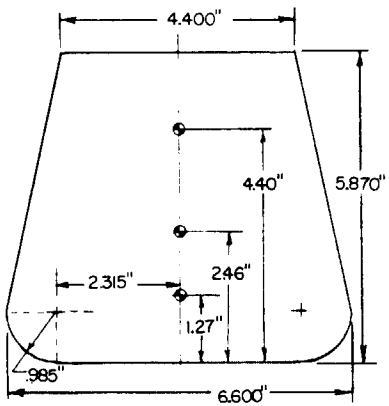

Model A

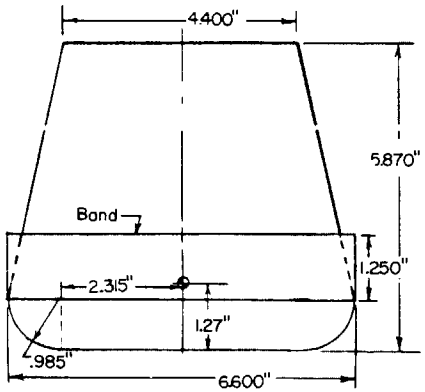

Model A with band Note: .5" band also used in one test; not shown in sketch.

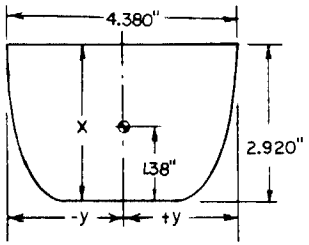

x, in.	±y, in.
0	0
.0073	1.1026
.0146	1.1820
.0365	1.2969
.0457	1.3267
.0913	1.4247
.1370	1.4863
.1825	1.5323
.2282	1.5694
.2738	1.6009
.3195	1.6283
.3650	1.6529
.4107	1.6764
.4563	1.6968
.5475	1.7317
.7300	1.7929
.9125	1.8437
1.0950	1.888
1.278	1.9276
1.4600	1.9641
1.643	1.9976
1.825	2.0293
2.0075	2.0589
2.1900	2.0871
2.373	2.1141
2.555	2.1407
2.738	2.1659
2.920	2.19

Model B

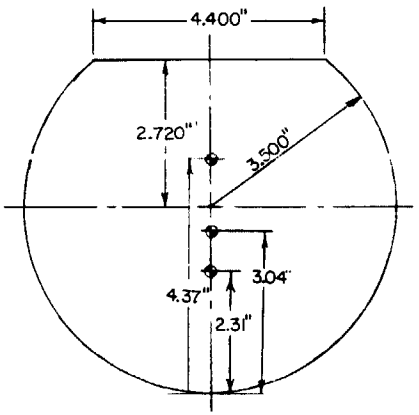

Model C

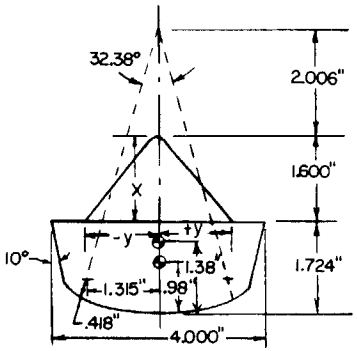

x, in.	±y, in.
0	1.38
0.1	1.28
0.2	1.23
0.3	1.10
0.4	1.03
0.5	0.95
0.6	0.88
0.7	0.80
0.8	0.75
0.9	0.65
1.0	0.57
1.1	0.49
1.2	0.42
1.3	0.34
1.4	0.26
1.5	0.18
1.6	0

Model D

Figure 4.- Sketches of models tested in Langley 20-foot free-spinning tunnel.

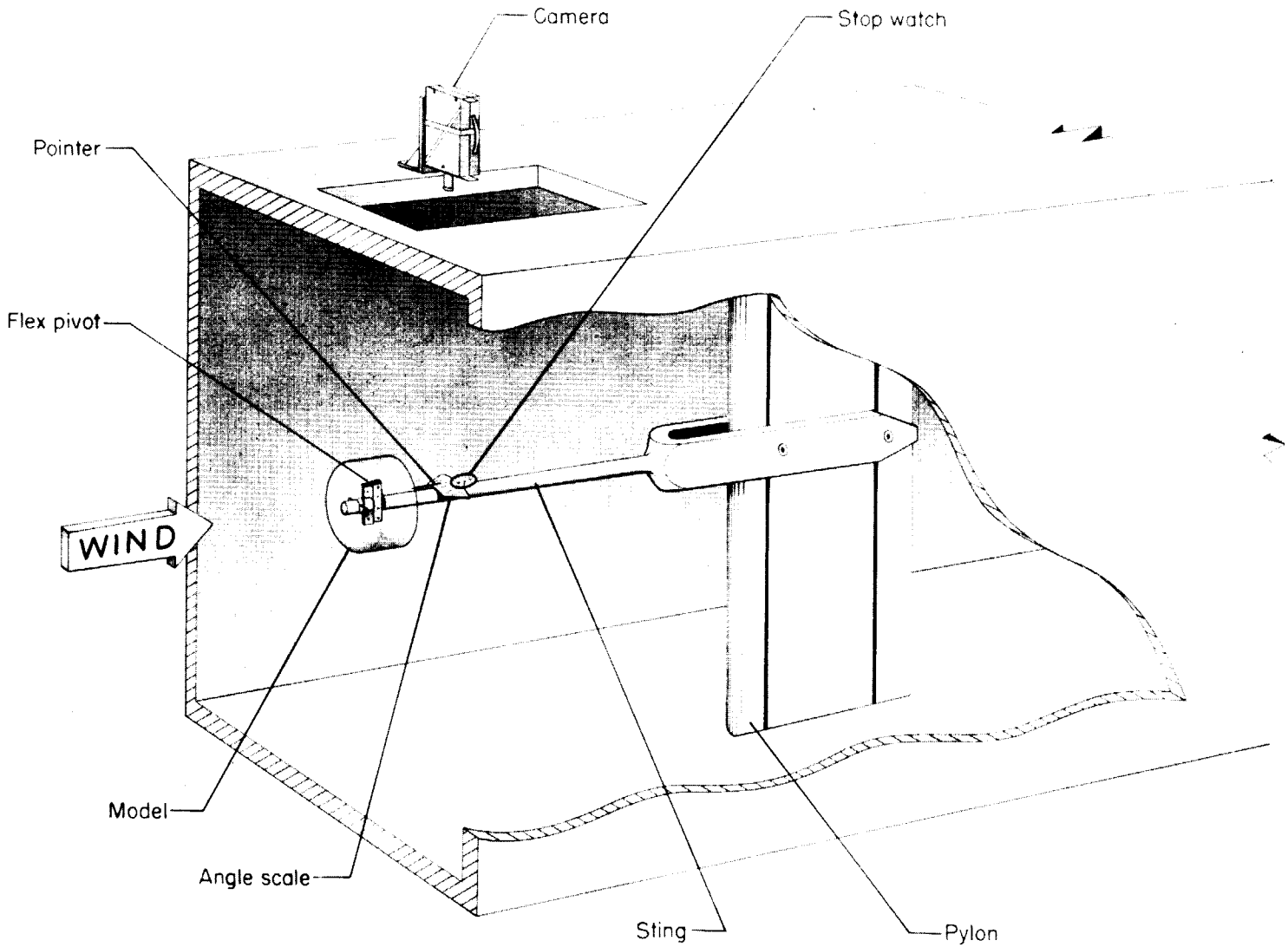

Figure 5.- Setup used in Langley stability tunnel for oscillation tests.

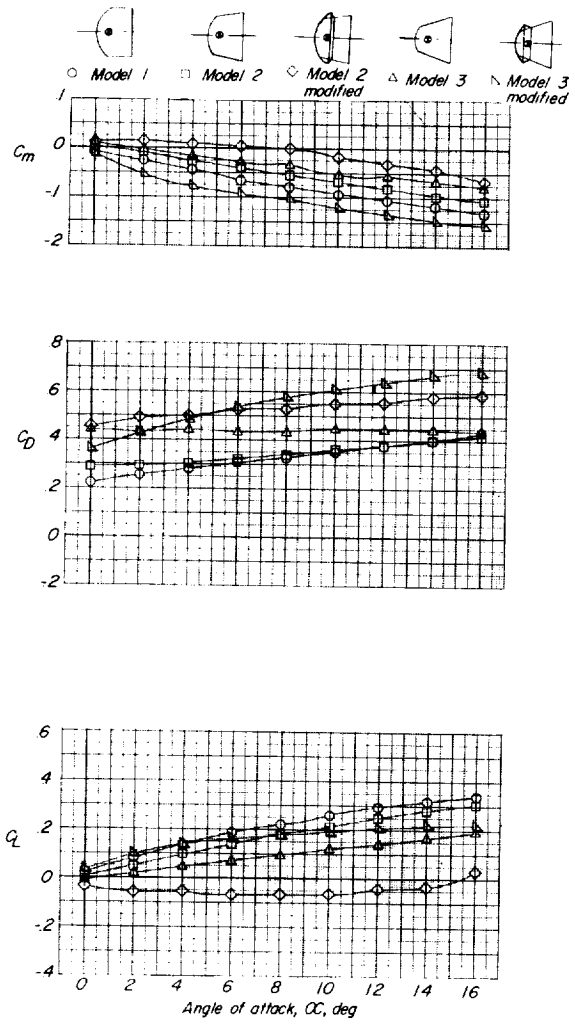

(a) Variation of C_L, C_D, and C_m with α for models 1, 2, and 3, and waist modifications on models 2 and 3.

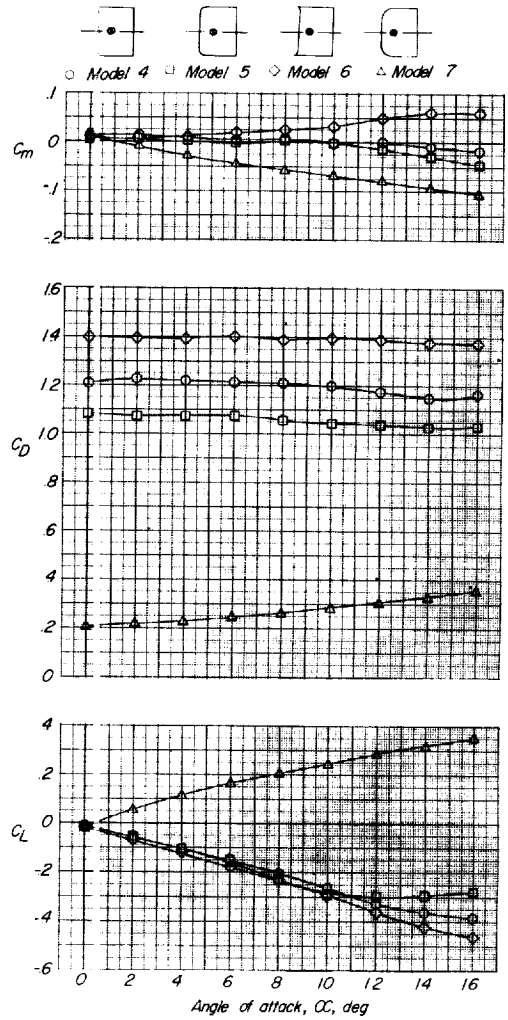

(b) Variation of C_L, C_D, and C_m with α for models 4, 5, 6, and 7.

Figure 6.- Variation of lift, drag, and pitching-moment coefficient with angle of attack, obtained from the static tests for models 1 to 7.

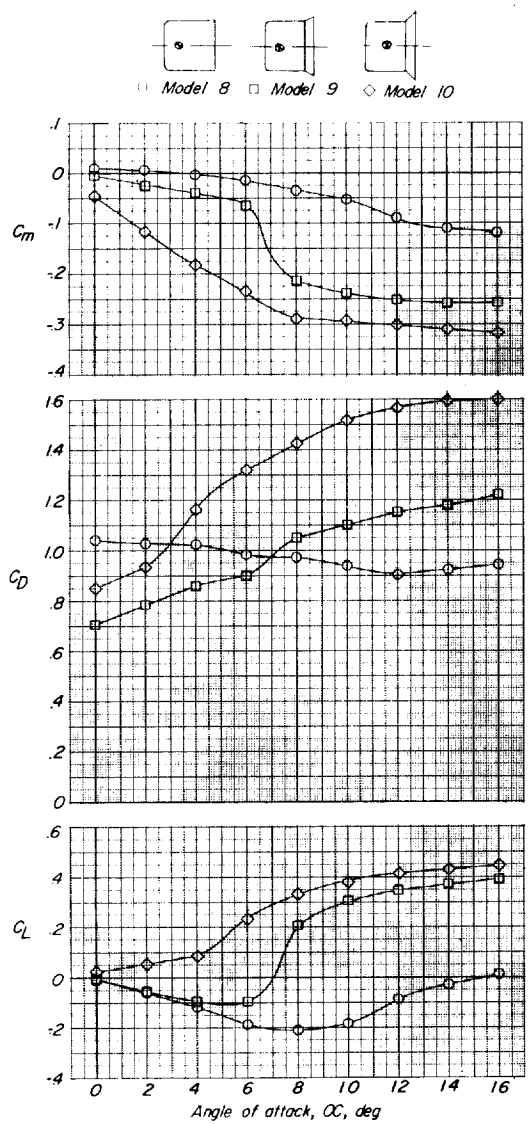

(a) Variation of C_L, C_D, and C_m with α for models 8, 9, and 10.

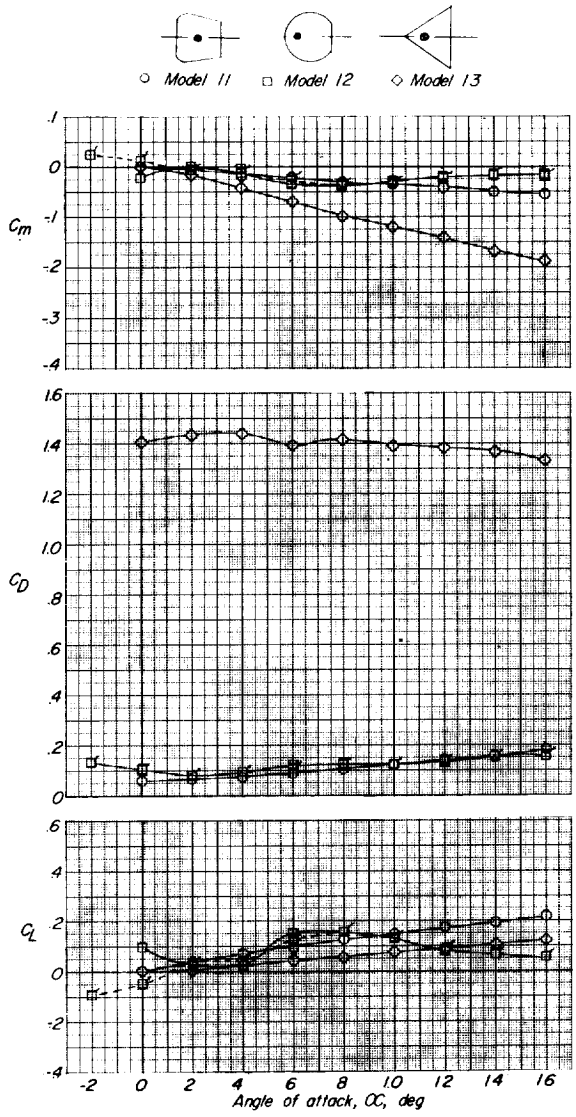

(b) Variation of C_L, C_D, and C_m with α for models 11, 12, and 13. Flagged symbols indicate duplication of an original test.

Figure 7.- Variation of lift, drag, and pitching-moment coefficient with angle of attack, obtained from static tests for models 8 to 13.

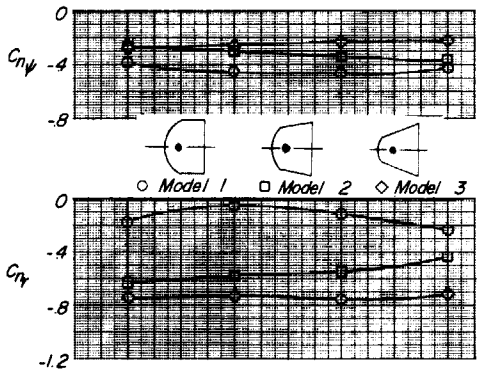

(a) Data for models 1, 2, and 3. Back closed. Center of gravity at 0.334l.

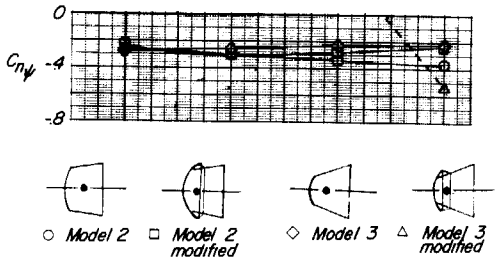

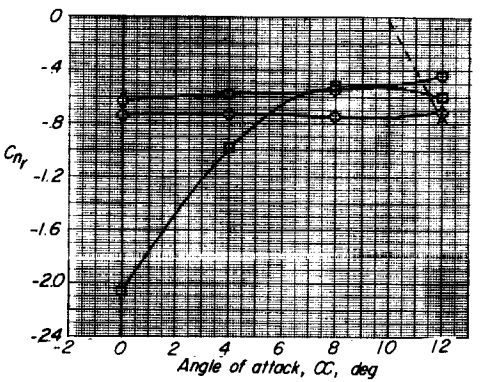

(b) Effect of waist modification on models 2 and 3. Back closed. Center of gravity at 0.334l.

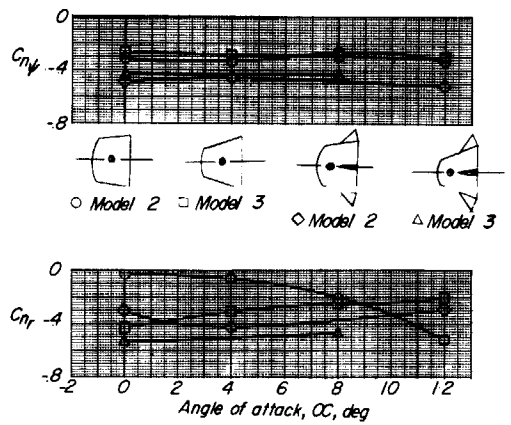

(c) Effect of tail fins on models 2 and 3. Back open. Center of gravity at 0.334l.

Figure 8.- Variation of static stability and damping derivatives with angle of attack, obtained from oscillation tests for models 1, 2, and 3.

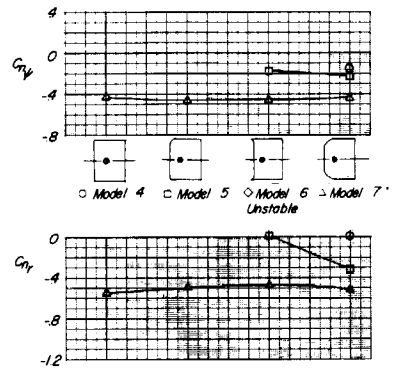

(a) Effect of nose corner radius. Models 4 to 7. Back closed. Center of gravity at 0.334l.

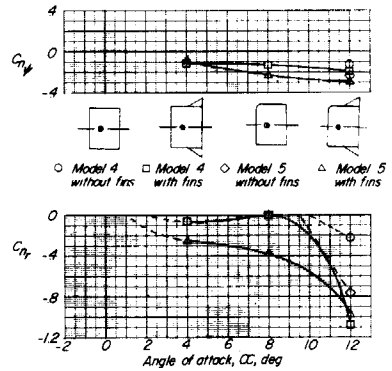

(b) Effect of fins on models 4 and 5. Back open. Center of gravity at 0.334l.

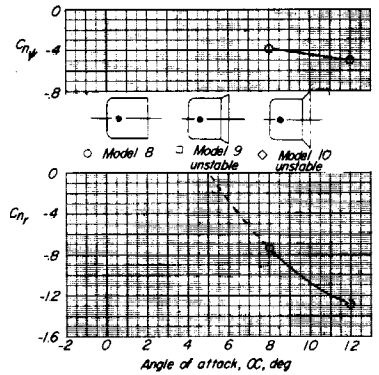

(c) Effect of skirt flare. Models 8, 9, and 10. Back closed. Center of gravity at 0.267l.

Figure 9.- Variation of static stability and damping derivatives with angle of attack, obtained from oscillation tests for models 4 to 10.

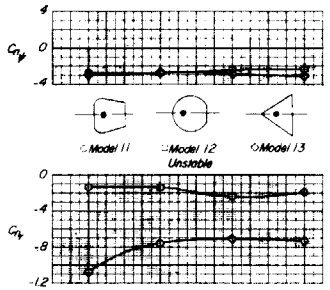

(a) Data for models 11, 12, and 13. Back closed. Center of gravity at 0.287l for models 11 and 12 and at 0.456l for model 13.

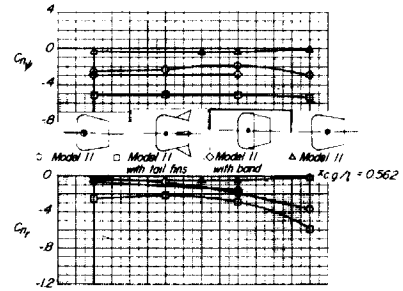

(b) Effect of center-of-gravity location and modification on model 11. Back open. Center of gravity at 0.287l except as indicated.

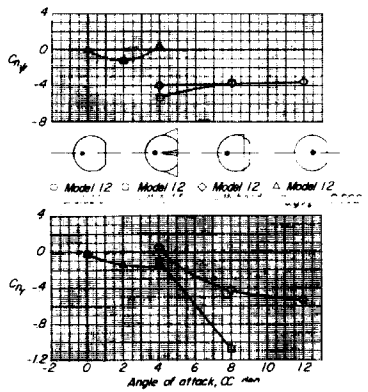

(c) Effect of center-of-gravity location and modification on model 12. Back open. Center of gravity at 0.287l except as indicated.

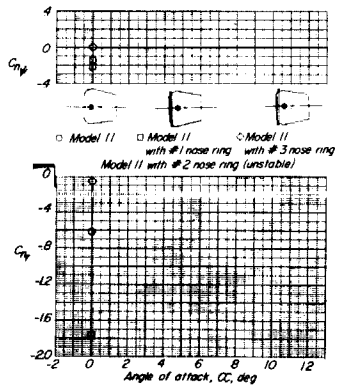

(d) Effect of nose ring on model 11 and 12. Back open. Center of gravity at 0.287l.

Figure 10.- Variation of static stability and damping derivatives with angle of attack, obtained from oscillation tests for models 11 to 13.